Domain-wall kinetics and tunneling-induced instabilities in superlattices

S. H. Kwok*
The Harrison M. Randall Laboratory of Physics, The University of Michigan, Ann Arbor, Michigan 48109-1120 and Center for Ultrafast Optical Science, The University of Michigan, Ann Arbor, Michigan 48109-2099

T. B. Norris
Center for Ultrafast Optical Science, The University of Michigan, Ann Arbor, Michigan 48109-2099

L. L. Bonilla, J. Galán,† J. A. Cuesta, F. C. Martínez, and J. M. Molera
Escuela Politécnica Superior, Universidad Carlos III de Madrid, Butarque 15, 28911 Leganés, Spain

H. T. Grahn and K. Ploog
Paul-Drude-Institut für Festkörperelektronik, Hausvogteiplatz 5-7, D-10117 Berlin, Germany

R. Merlin
The Harrison M. Randall Laboratory of Physics, The University of Michigan, Ann Arbor, Michigan 48109-1120 and Center for Ultrafast Optical Science, The University of Michigan, Ann Arbor, Michigan 48109-2099
(Received 17 November 1994)

We report on time-resolved studies of electric-field domains in weakly coupled GaAs quantum-well structures. Photoluminescence and photocurrent experiments probe the motion of charged domain walls triggered by steplike changes in the illumination. Results reveal complex oscillations with frequencies in the range 4–8 MHz. These findings are discussed in terms of a discrete drift model relying on negative-differential conductance due to resonant tunneling. Calculations give a global phase diagram and time behavior consistent with experiments.

Central to the transport behavior of semiconductor superlattices (SL's) is the question of the mechanisms of negative differential conductance and associated instabilities.[1,2] This problem bears on phenomena as diverse as Bloch oscillations[3] and Wannier-Stark ladders,[4] as well as on various aspects of nonlinear dynamics[5] and resonant tunneling.[6–8] A related but distinct question is that of the transitions between different transport modes. As has been known for quite some time, SL's may spontaneously break into regions referred to as electric-field domains (EFD's) so that the field is not uniform but piecewise constant across the sample.[9–19] However, the nature of the instability and that of the parameters which control the transition have remained largely unexplained. In this Brief Report, we provide the solution to this problem.

Domains are specific to the quantum-well (QW) regime of small miniband widths. For weakly coupled SL structures, transport is dominated by sequential resonant tunneling.[6–8] At low carrier densities, the I-V (current-voltage) response is of the form shown in Fig. 1(a) with maxima at fields $\mathcal{E}_{ij}(i,j \geq 1)$ corresponding to the neighboring-well alignment of the ith and jth subbands.[8] In 1974, Esaki and Chang[7] reported conductance data leading to traces such as the one illustrated in Fig. 1(b), which reflect the presence of microscopic EFD's.[9–19] Recently, it has become clear that the dependence shown in Fig. 1(b) corresponds to the high-density limit.[13] Here we study the transition between the EFD and the uniform-field regime by monitoring the time behavior of a photoexcited QW system as it evolves from (a) to (b). We also present theoretical results which account for both the steady-state and time-domain data. A detailed description of the procedures used in this work will be given elsewhere.[20,21]

The QW structure used in our experiments was characterized in Refs. 17 and 18. It consists of $N=40$ periods of nominally undoped GaAs wells and AlAs barriers of widths 90 and 40 Å, respectively, sandwiched between heavily donor- and acceptor-doped $Al_{0.5}Ga_{0.5}As$ layers giving diodes which were processed into mesas of area ~ 0.01 mm^2; the built-in voltage of the devices is ≈ 1.5 V. Because the superlattice is not purposely doped, the I-V response in the low carrier density limit is of the form shown in Fig. 1(a).[18] Under strong photoinjection of carriers, however, the samples exhibit EFD's with I-V traces such as that shown in the inset of Fig. 2.[17,18] Here the plateau region $+1.5\ \text{V} \lesssim V \lesssim -3.5$ V corresponds to coexisting domains $\mathcal{E}_{11}/\mathcal{E}_{12}$,[17] while the second plateau $-4.5\ \text{V} \lesssim V \lesssim -7.5$ V is due to $\mathcal{E}_{12}/\mathcal{E}_X$, where $\mathcal{E}_X$ denotes an unidentified domain (negative signs denote reverse bias). Our experiments, focusing on the higher plateau, probe the transient behavior of the QW's as they evolve from the regime of uniform field to that of domains. For this, the photoexcitation was turned on and off by switching a Pockels cell placed between crossed polarizers; our setup gives steplike profiles with rise times of ≈ 5 ns at a repetition rate of 3.5 kHz. Time-resolved data at $T=18$ K were obtained with a

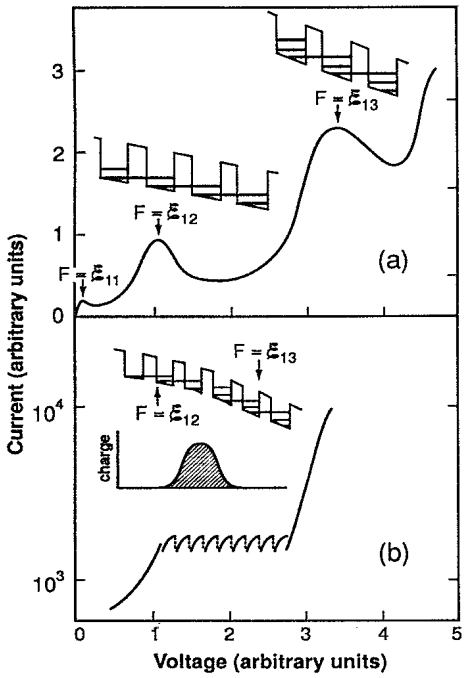

FIG. 1. Schematic I-V traces corresponding to (a) uniform-field (low density) and (b) domain regimes (high density). The current maxima in (a) are due to tunneling involving the level alignment shown in the figure. In (b), the ratchetlike structure reflects the motion of the wall by one superlattice period (Ref. 2); the inset depicts the z dependence of the potential and charge in the vicinity of the domain boundary.

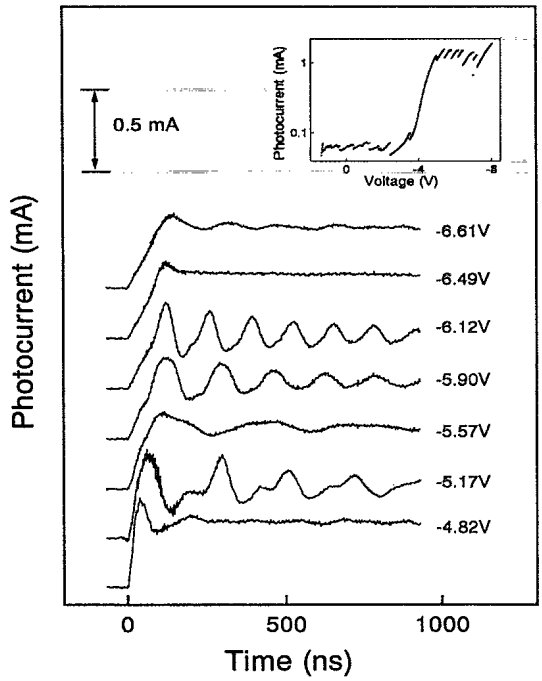

FIG. 2. Measured photocurrent vs time at $T=18$ K, offset vertically for clarity. The voltages are in the range where domains $\mathcal{E}_{12}$ and $\mathcal{E}_X$ coexist. Photoexcitation ($P=250$ W cm^{-2}, $\lambda=6540$ Å) begins at $t=0$. The inset shows the experimental steady-state dependence of the photocurrent on the applied bias at $\lambda=6471$ Å, $P=10^3$ W cm^{-2}, and $T=4$ K.

Tektronix 1-GHz sampling oscilloscope (model 11402). The photocurrent (PC) was inferred from the voltage across a 50-Ω series resistor. Band-gap photoluminescence (PL) served to monitor the field profile through the quantum-confined Stark effect;[22] the emission shifts to the red with increasing field. PL spectra were obtained at a resolution of ~9 Å, by recording the output of a photomultiplier sampled by the oscilloscope. As a light source, we used a dye laser operating at $\lambda=6500$–6600 Å. Power densities were in the range $P=30$–300 W cm^{-2}, leading to EFD's in the steady state;[18] signals were unacceptably low at smaller powers. As the photoexcitation energies (~1.90 eV) are well above the QW gap at ~1.56 eV, the data do not depend much on λ.

Typical results of PC and PL vs time (t) are shown in Figs. 2 and 3. Following the onset of photoexcitation at $t=0$, the current exhibits *damped* oscillations characterized by parameters depending on V; see below. At a fixed bias, the P dependence of the current (not shown) reveals that the oscillations exist only in a narrow window of intensities, so that the PC becomes a simple step function if P is either too high or too low; in addition, the fundamental frequency Ω depends significantly on P. The PL data of Fig. 3 show a single feature at $t=0$ which splits into two peaks. For $t \gtrsim 100$ ns the intensities of these peaks oscillate with time, but their positions do not vary much. At a given bias, the latter agree well with values from steady-state spectra. The V dependence of Ω is shown in the inset of Fig. 3. It exhibits several minima as well as discontinuities which appear to correlate with those of the steady-state photocurrent (Fig. 2, inset); the decay time (≈ 0.2–0.5 μs) shows a similar trend. Given P and V, the frequencies determined from PC and PL measurements are the same within experimental error.

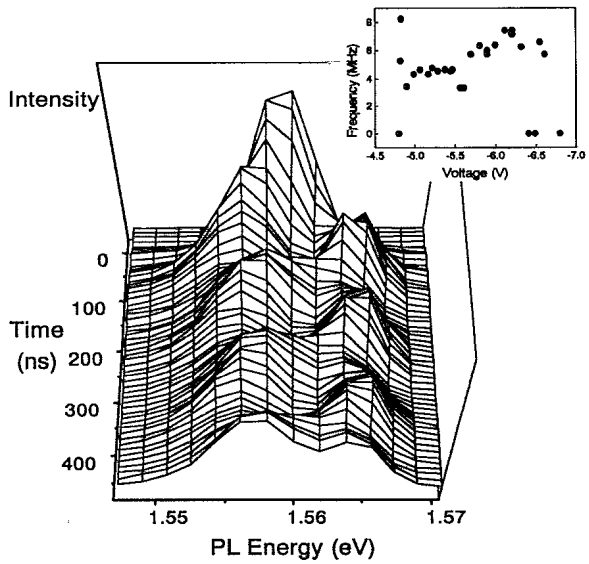

FIG. 3. Experimental time-resolved PL data at $V=-6.21$ V. Spectra are given at intervals of 10 ns. The oscillating peaks at ≈ 1.557 and ≈ 1.565 eV correspond, respectively, to the high- ($\mathcal{E}_X$) and low-field ($\mathcal{E}_{12}$) domains. The V dependence of the fundamental oscillation frequency is shown in the inset. Data were obtained at $\lambda=6540$ Å, $P=250$ W cm^{-2}, and $T=18$ K.

In our sample, the oscillatory behavior is limited to the range of $\mathcal{E}_{12}/\mathcal{E}_X$ coexistence. For these voltages, steady-state PL spectra show two Stark-shifted peaks associated with $F \approx \mathcal{E}_{12}$ (low field) and $\mathcal{E}_X$ (high field).[17] While the peak energies depend only weakly on V, the low-field (high-field) intensity decreases (increases) rapidly with increasing bias, following the movement of the domain boundary. Thus steady-state PL vs V across the plateau resembles the t-dependent data during half a cycle, indicating that the displacement of the wall with voltage and the oscillation with time are similar in nature. As mentioned above, the PL positions determined from steady-state and time-resolved measurements (at $t \gtrsim 0.1$ μs) are roughly the same. Based on this, we ascribe the damped oscillations to the back and forth motion of the domain boundary approaching equilibrium. Notice that our results are inconsistent with the scenario dominated by the charging and discharging of a stationary wall; this would have led to time-varying energy shifts as opposed to oscillating intensities. The domain walls form within 50–100 ns after the laser is turned on. Interestingly, PL experiments at the $\mathcal{E}_{11}/\mathcal{E}_{12}$ plateau failed to reveal either EFD's or oscillations for $t < 1$ μs (the quality of our laser step profile deteriorates rapidly after $\approx 1-1.5$ μs); this value represents a lower limit for the corresponding boundary formation time.

Our discrete drift model, differing from other proposals[16,19] in various respects,[23] considers a set of weakly interacting QW's characterized by average values of the electric field, F_k, and carrier densities, n_k (electrons) and p_k (holes); $k = 1, \ldots, N$ labels the wells. Such mean-field-like approach is motivated by the fact that the relevant time for oscillations (≈ 0.1 μs) is considerably larger than those for tunneling (≈ 0.5 ns) and for reaching equilibrium with the lattice (≈ 10 ps).[24] The one-dimensional transport equations read

$$F_k - F_{k-1} = \frac{4\pi e l}{\epsilon_0}(n_k - p_k) , \tag{1}$$

$$\epsilon_0 \frac{dF_k}{dt} + e\nu(F_k) n_k = J , \tag{2}$$

$$\frac{dp_k}{dt} = \gamma - r n_k p_k , \tag{3}$$

where (1) and (2) are, respectively, the Poisson equation and Ampère's law; (3) is the hole rate equation containing the photogeneration rate γ (proportional to the laser power-density), and the recombination constant r. The superlattice period and dielectric constant are denoted by l and ϵ_0. $\nu(F)$ is an effective electron velocity and J is the current density. The rate equation for electrons can be obtained by differentiating (1) and using (2) and (3). Notice that the contribution of the heavier holes to the current is ignored.

Much of the physics of the model is contained in $\nu(F)$, which we take as a datum while making the assumption that it does not depend on density. Qualitatively, our results do not depend on the precise shape of $\nu(F)$ provided the function exhibits maxima at the resonant fields; the calculations reported here are based on the curve shown in the inset of Fig. 4. In the $3N$ equations (1)–(3), there

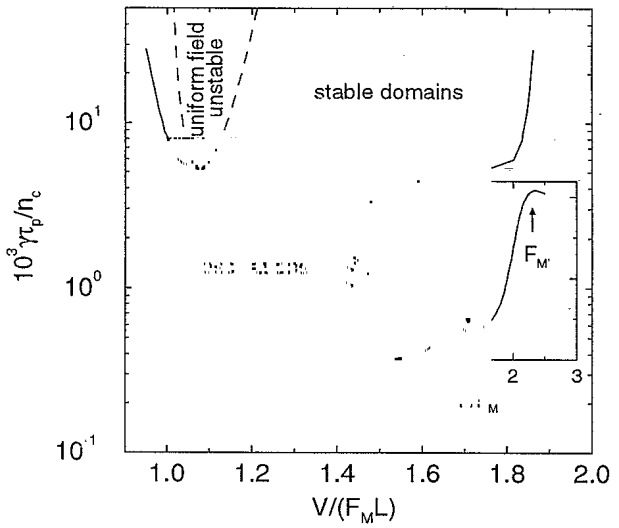

FIG. 4. Theoretical phase diagram of the photogeneration rate γ vs applied voltage V in units of, respectively, n_C/τ_p and $F_M L$; see text. The shaded region denotes the approximate range of domain-wall oscillations. The continuous (dotted) curve delimits the region for which the domain (uniform-field) solution is stable (unstable). Inset: The normalized field dependence of the carrier velocity used as input in the calculations.

are $3N+2$ unknowns. To solve the problem, we add the bias equation $\sum F_k = V/l$ and the boundary condition $n_1 = p_1$, not allowing for charge buildup at the first well.[20] In the analysis, it is convenient to render the equations dimensionless by adopting as the units of field and velocity the values at the first maximum of $\nu(F)$, F_M, and ν_M (see Fig. 4, inset). Further, we express the carrier density and bias in terms of $n_c = \epsilon_0 F_M/(4\pi e l)$ and $F_M L$, with $L = Nl$. This yields the time and current units $\tau_p = (r n_c)^{-1}$ and $J_M = e\nu_M n_c$. In our sample $n_c \sim 5.5 \times 10^{17}$ cm^{-3} and $F_M L \sim 5.2$ V, and we estimate $\tau_p \sim 10$ ns [note that r and, thus, τ_p depend on F (Ref. 25)]. As discussed below, τ_p determines the time scale of

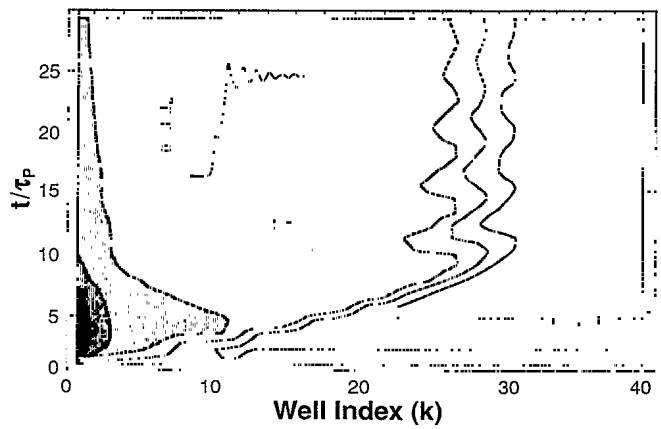

FIG. 5. Calculated contour plot of F/F_M as a function of t/τ_p and the quantum-well index k for $\gamma\tau_p/n_C = 2\times 10^{-3}$ and $V/(F_M L) = 1.2$; the contour spacing is 0.2. Notice that the field is uniform at $t = 0$. Domains are already defined at $t \approx 5\tau_p$, and the wall oscillates for $t \gtrsim 10\tau_p$. The theoretical time dependence of the normalized current density, J/J_M, is shown in the inset.

the oscillations.

Stationary solutions to (1)–(3) follow a discrete mapping of the form $F_{k-1}=f(F_k;\gamma,J)$ which, depending on the parameters, has either one or three fixed points.[20] The latter is a necessary condition for EFD's. Let F_m and $F_{M'}$ be as in the inset of Fig. 4. For voltages between the two maxima, we find nonuniform solutions with fields $\mathcal{E}_L$ and $\mathcal{E}_H$ separated by a domain wall. The fields are such that $\mathcal{E}_L<F_M$ (or $F_M<\mathcal{E}_L<F_m$) and $F_m<\mathcal{E}_H<F_{M'}$,[20] in agreement with data reported in Ref. 18. Using linear stability analyses, we determined the region shown in Fig. 4 for which the EFD (uniform field) is stable (unstable). In general, there are two or more solutions at a given V with a similar field profile, but with the wall displaced by one or more wells. Consistent with experiments, this gives rise to hysteresis and flat, ratchetlike I-V traces similar to that in Fig. 1(b). The magnitude of these effects increases with increasing γ.[20]

To extract time-dependent magnitudes from our model, we solved (1)–(3) using standard numerical methods.[20] In the simulations, we fix V and let the system evolve after the illumination is turned on at $t=0$. Theory agrees with experiments in that oscillations of period $\sim O(\tau_p)$ exist for voltages corresponding to $\partial v/\partial F<0$ (see Fig. 4). The oscillatory behavior is found in a γ window comprising stable but also unstable ($\gamma\tau_p/n_C<5\times10^{-3}$) stationary domains. The experiments obey the prediction that there are no oscillations at large powers where the system becomes overdamped. Typical results for $F(t)$ and $J(t)$ are shown in Fig. 5. As anticipated, the calculations clearly identify the origin of the oscillations as due to the movement of the EFD boundary. This motion leads to current vs t traces like the one in the inset. Qualitatively, the theoretical V and γ dependences of the frequency (not shown) agree well with the measurements, in that Ω varies by at most a factor of 2 in the oscillatory range.

This work was supported by the U.S. Army Research Office under Contract No. DAAL-03-92-G-0233, and the National Science Foundation through the Center for Ultrafast Optical Science under STC PHY 8920108; the Bunderministerium für Forschung und Technologie of Germany; the EC Human Capital and Mobility Programme under Contract No. ERBCHRXCT930413; and DGICyT of Spain under Grant Nos. PB92-0248 and PB91-0378.

*Present address: Paul-Drude-Institut für Festkörperelektronik, Hausvogteiplatz 5-7, D-10117 Berlin, Germany.
†Present address: Department of Physics, The Ohio State University, Columbus, OH 43210.

[1]L. Esaki and R. Tsu, IBM J. Res. Dev. **14**, 61 (1970).
[2]A. Sibille *et al.*, Phys. Rev. Lett. **64**, 52 (1990); X. L. Lei, N. J. M. Horing, and H. L. Cui, *ibid.* **66**, 3277 (1991).
[3]See, e.g., C. Waschke *et al.*, Phys. Rev. Lett. **70**, 3319 (1993).
[4]J. Bleuse, G. Bastard, and P. Voisin, Phys. Rev. Lett. **60**, 220 (1988); E. E. Mendez, F. Agulló-Rueda, and J. M. Hong, *ibid.* **60**, 2426 (1988); K. H. Schmidt *et al.*, *ibid.* **72**, 2769 (1994).
[5]See *Proceedings of the NATO Advanced Research Workshop on Negative Differential Resistance and Instabilities in 2D Semiconductors,* Vol. 307 of *NATO Advanced Study Institute, Series B: Physics,* edited by N. Balkan, B. K. Ridley, and A. J. Vickers, (Plenum, New York, 1992).
[6]R. F. Kazarinov and R. A. Suris, Fiz. Tekh. Poluprovodn. **6**, 148 (1972) [Sov. Phys. Semicond. **6**, 120 (1972)].
[7]L. Esaki and L. L. Chang, Phys. Rev. Lett. **33**, 495 (1974).
[8]F. Capasso, K. Mohammed, and A. Y. Cho, Appl. Phys. Lett. **48**, 478 (1986).
[9]Y. Kawamura, K. Wakita, and K. Oe, Jpn. J. Appl. Phys. **26**, L1603 (1987).
[10]K. K. Choi *et al.*, Phys. Rev. B **38**, 12 362 (1988), and references therein.
[11]T. H. H. Vuong, D. C. Tsui, and W. T. Tsang, Appl. Phys. Lett. **52**, 981 (1988).
[12]M. Helm *et al.*, Phys. Rev. Lett. **63**, 74 (1989).
[13]H. T. Grahn *et al.*, Phys. Rev. B **41**, 2890 (1990).
[14]H. T. Grahn *et al.*, Phys. Rev. Lett. **67**, 1618 (1991).
[15]A. Shakouri *et al.*, Appl. Phys. Lett. **63**, 1101 (1993).
[16]B. Laikhtman and D. Miller, Phys. Rev. B **48**, 5395 (1993); D. Miller and B. Laikhtman (unpublished).
[17]H. T. Grahn *et al.*, Surf. Sci. **267**, 579 (1992).
[18]S. H. Kwok *et al.*, Phys. Rev. B **50**, 2007 (1994).
[19]F. Prengel, A. Wacker, and E. Schöll, Phys. Rev. B **50**, 1705 (1994).
[20]L. L. Bonilla *et al.*, Phys. Rev. B **50**, 8644 (1994).
[21]S. H. Kwok *et al.* (unpublished).
[22]See, e.g., D. A. B. Miller *et al.*, Phys. Rev. Lett. **53**, 2173 (1984).
[23]Unlike our approach, Ref. 16 deals with an infinitely long SL using $F\approx\mathcal{E}_{12}$ as a boundary condition and ignoring the holes. At high densities, our theory is nearly equivalent to that of Ref. 19 (doped SL's) in the limit where the intrawell relaxation time vanishes. However, note that Prengel, Wacker, and Schöll (Ref. 19) [as well as Laikhtman and Miller (Ref. 16)] consider primarily $\mathcal{E}_{11}/\mathcal{E}_{12}$ coexistence and do not address the question of the transition between EFD and the uniform-field regime.
[24]See, e.g., J. Shah, *Hot Carriers in Semiconductor Nanostructures: Physics and Applications* (Academic, Boston, 1992), p. 279.
[25]H.-J. Polland *et al.*, Phys. Rev. Lett. **55**, 2610 (1985).